ISSN 1392-3730/eISSN 1822-3605

VILNIUS TECH
Vilnius Gediminas Technical University

JOURNAL of CIVIL ENGINEERING and MANAGEMENT

2024
Volume 30
Issue 7
Pages 566–580
https://doi.org/10.3846/jcem.2024.21743

NUMERICAL SIMULATION ANALYSIS OF CONTROLLING SETTLEMENT BY WATER-RESISTING CURTAIN COMBINED WITH RECHARGE IN DEEP FOUNDATION PIT

Xubing XU[1], Yonglai ZHENG[1], Xin LAN[1]✉, Jie PAN[2], Yuan WEN[1]

[1] *Civil Engineering College, Tongji University, Shanghai, 200092, China*
[2] *Wuxi Survey and Design Institute Co. Ltd., Jiangsu, 214072, China*

Article History:
- received 28 December 2023
- accepted 4 April 2024

Abstract. This study takes a nearby foundation pit project of a high-speed railway in Yancheng City, Jiangsu Province as an example to investigate the impact of deep foundation pit projects on groundwater and the surrounding environment. Through on-site monitoring, in-situ testing, and numerical simulation, we conducted a comprehensive study of the impact of foundation pit projects on groundwater and the surrounding environment. The evolution of groundwater levels and surface displacement during the excavation of foundation pits was analyzed, and a method for measuring the permeability of target soil layers in situ was studied. The simulation of recharge under various soil conditions was performed, and the outcomes demonstrated the effective isolation of hydraulic connections between the interior and exterior of the foundation pit by the water-resistant curtain. Precipitation head and constant head recharging tests were employed to ascertain the actual permeability. The characteristic time method calculation exhibited remarkable efficiency and accuracy in determining the permeability coefficient of the recharging soil layer. Recharging phreatic and confined water layers has differing degrees of influence on surface deformation, with the impact of confined water layers requiring more time to stabilize. These findings contribute significantly to a more comprehensive understanding of the environmental repercussions associated with deep excavation projects, thereby enhancing safety and environmental protection measures in excavation construction practices.

Keywords: confined water, water-resisting curtain, recharging, excavation of foundation pit, numerical simulation.

✉Corresponding author. E-mail: *2410024@tongji.edu.cn*

1. Introduction

As deep excavation projects continue to expand in terms of size and depth, their impact on the surrounding environment becomes a critical concern. In areas with high groundwater levels, deep excavation projects often employ dewatering during excavation or implement water-resisting curtains to enhance construction safety. However, in addition to the potential ground deformation caused by earthwork excavation and subsequent construction processes of deep excavation projects (Wang et al., 2010), pre-excavation dewatering can also lead to the deformation of the support system and surrounding soil masses (Zeng et al., 2018). To mitigate the environmental impact of deep excavation on its surroundings, it is common practice to install recharge wells on the outer periphery of the excavation. These wells serve to compensate for groundwater loss, thereby controlling surface settlement (Guo et al., 2022; Mohammadzadeh-Habili & Khalili, 2020; Zhang et al., 2017; Zheng et al., 2022).

In foundation pit engineering, the role of environmental conditions and displacement monitoring in the vicinity of the pit is of paramount importance. Monitoring serves to prevent geological hazards, ensuring the safety of surrounding structures and underground facilities (Roy & Robinson, 2009), while also allowing for timely adjustments in construction strategies to mitigate potential risks (Jan et al., 2002). Through a three-dimensional surface deformation monitoring of a 12.8-meter deep excavation project in Chicago, Finno and Roboski (2005 and Finno et al. (2007) summarized ground responses during excavation and proposed a performance-based approach to estimate the maximum horizontal ground movement of flexible wall systems. By monitoring and comparing multiple cases of deep excavations in soft soil near subway stations, reasonable phased excavation can effectively minimize the impact on the surrounding environment and reduce ground surface settlement during excavation (Chen

et al., 2016; Ding et al., 2018; Li et al., 2017). Earthwork excavation and support removal can result in the settlement of support pile caps, structural columns, and adjacent ground, but cushion layer construction can mitigate pit deformation. Foundation pit excavation primarily affects subway tunnel settlement, with rapid initial deformation increase, which gradually diminishes with increasing distance from the excavation area (Song et al., 2020). Sun and Xiao (2021) explored deformation characteristics in foundation pit engineering through field monitoring and model experiments. Results indicated a linear reduction in sidewall displacement as the distance between pits increased, but an increase in the width of internal pit excavation led to larger displacements. Chen et al. (2022) conducted environmental monitoring around a cluster of deep foundation pits and found that adjacent pit excavation reduced lateral deformation of retaining piles while causing soil uplift. By optimizing the excavation sequence of the pit cluster, they successfully controlled the deformation associated with this unique excavation scenario.

Numerical simulations of foundation pit engineering enable the prediction of groundwater level fluctuations, soil deformations, and the stress experienced by retaining structures (Faheem et al., 2004; Finno et al., 2007; Schäfer & Triantafyllidis, 2006). These simulations aid in devising support schemes, reducing risks, ensuring construction safety, and safeguarding neighboring buildings and underground facilities (Hou et al., 2008; Son & Cording, 2008; Zheng & Wei, 2008). Taking the dewatering project at Hangzhong Road Station of Shanghai Metro Line 10 as a case, Zhou et al. (2010) employed numerical simulations to determine the control effect of increasing the depth of continuous concrete walls on dewatering. Combining numerical simulation analysis, a construction scheme employing pile-plate retaining walls along with ground treatment was proposed for open-cut tunnel construction (Liu et al., 2011). It was found that, under conditions of smaller excavation volume, the uplift of existing tunnels exhibited nonlinear growth with increasing excavation width for each step. Utilizing the phased excavation method minimized tunnel uplift, effectively controlling the uplift range. Dong et al. (2014) investigated a deep foundation pit project at the North Square Shopping Center of Shanghai South Station. They conducted comprehensive monitoring during construction and calibrated numerical analyses using field data. Liao et al. (2016) employed numerical simulations to study the influence of excavation depth and distance on subway station deformation and internal structural stress. The results demonstrated a close alignment between simulation outcomes and field observations of the subway station. Furthermore, Tong et al. (2021) conducted numerical simulations to probe into the influence mechanism of complex foundation pit excavation based on nested pits on the lateral response of piles in the transition zone and then introduced an assessment method that unveiled the impact pattern of inner pit excavation on the lateral bearing performance of piles. The practical problems faced by underground rock and soil engineering are unique and stochastic, so relatively lagging theoretical research cannot guide the rapid development of large-scale high-speed construction. Existing theories need significant adjustments when applied to actual engineering, based on experience and site conditions. Therefore, when facing similar problems, qualitative analysis based on past engineering experience is often used, lacking reliable quantitative theoretical analysis as the basis for guiding engineering practices.

This study, using a foundation pit engineering project located near a high-speed railway in Yancheng City, Jiangsu Province, as a case study, employed various methods such as field monitoring, in-situ recharging tests, and numerical simulations. It analyzed the characteristics and patterns of changes in groundwater and surface displacements during the excavation of the foundation pit. Additionally, the study explored an in-situ testing method that allows for the rapid determination of the permeability of the target soil layer. The feasibility of recharging simulations under multi-layer soil conditions was verified through numerical modeling. Furthermore, the study analyzed the impacts on the surrounding environment when recharging was carried out separately for confined aquifers and pressurized aquifers outside the cutoff wall. This study provides the scientific basis and technical support for the non-dewatering construction of deep excavation projects, which helps improve the safety and efficiency of engineering construction, reduces the impact on the surrounding environment, and has certain engineering applications and promotion value.

2. Engineering background

2.1. Overview of the pit excavation project

This pit excavation project is a supporting project for a comprehensive hub of a high-speed railway station in Jiangsu. The foundation pit is adjacent to the high-speed Railway station and the Railway track. The nearest distance between the upper pit line and the foot of the slope of the Xinchang Railway is about 46 m, and the distance from the Yantong High-speed Railway line is about 105 m. This pit is a two-story basement, with the excavation depth varying from 10.2 to 12.0 m, and the excavated area of the pit is about 19677 m^2. Figure 1 shows the general layout of the site conditions.

This project is located in the coastal plain area of northern Jiangsu, China, forming a vast coastal plain geomorphic unit. The soil layers involved in the construction area are Late Pleistocene-Holocene Quaternary deposits. Through investigation, it was found that the geological structure stability of the site area is good, with no obvious adverse geological phenomena such as karst, landslides, dangerous rocks, collapse, debris flows, mining areas, or active faults. The overall stability of the site is good. The factors affecting the safety of the project and its surround-

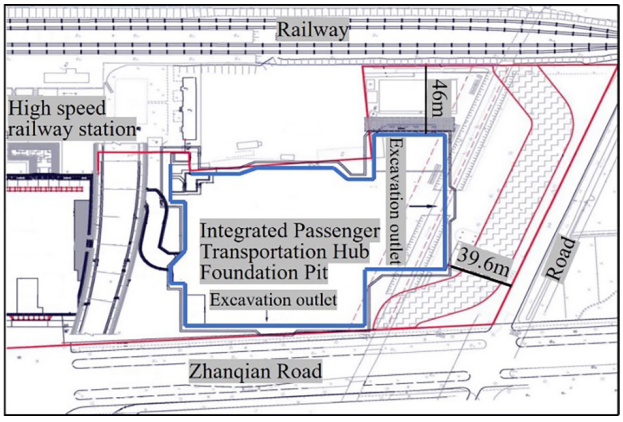

Figure 1. The overall plan of the foundation pit project site environment

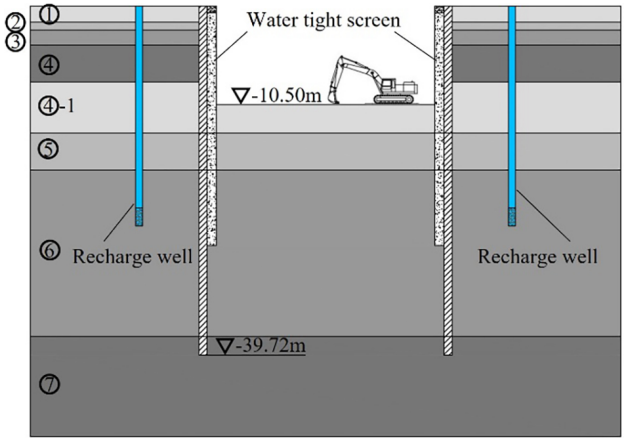

Figure 2. The stratum and foundation pit structure profile

ings include pore water and confined water. Among them, pore water mainly exists above the clay layer of the layer ⑤. Its influence mainly comes from climate precipitation and surface water recharge, and the water level varies with the seasons. Confined water mainly exists in the soil layer of the layer ⑥, and its recharge source is the lateral flow of the same aquifer. Based on the engineering survey report and indoor permeability coefficient tests, the vertical permeability coefficient, horizontal permeability coefficient, and soil layer composition are presented in Table 1. In compliance with relevant railway regulations, this project falls within the groundwater protection zone, and groundwater extraction is strictly prohibited. Drainage construction is achieved through the utilization of water-resisting curtains and open drainage systems inside the pit.

The foundation pit's retaining structure utilizes bored cast-in-situ piles with diameters ranging from Φ 1000 to 1200 mm, with some sections employing double-row piling. Inside the pit, a reinforced concrete support system is installed for structural reinforcement, consisting of diagonal bracing in conjunction with edge trusses. In consideration of the safety requirements for railway and high-speed railway operations, the construction of this foundation pit engineering project adopts a "non-dewatering" approach, which means that no dewatering wells are installed. Instead, it utilizes cutoff walls and in-pit drainage for dewatering purposes. The cutoff walls consist of double rows (with localized triple-row cutoff piles) of Φ 850 mm ultra-deep three-axis cement-mixing piles. Within the pit, drainage channels collect water, and drainage is facilitated through collection wells. At the bottom of the pit, high-pressure jet grouting piles are used for bottom sealing and reinforcement, reaching a depth of 5 meters below the pit bottom to ensure both soil stability and water-resisting curtaining. In the area of the post-pouring belt of the foundation pit, ultra-deep three-axis mixing piles are employed for partitioning, simultaneously serving as water barriers. Specific geological layers and cross-sections of the foundation pit structure are depicted in Figure 2.

2.2. Arrangement of measuring points

To ensure the safety of the foundation pit itself, the surrounding environment, and the continued safe operation of the railway system during construction, a comprehensive monitoring system was deployed within the foundation pit and its vicinity. This system encompasses monitoring water levels, surface subsidence, ring beam displacement, adjacent structure settlement, and railway subgrade settlement.

Table 1. Soil composition and permeability coefficient

Layer	Composition of each layer	H (m)	ρ (kg/m^3)	k_v (m/s)	k_h (m/s)
①	Miscellaneous fill	0.5~0.8	1760	5.0×10^{-6}	5.0×10^{-6}
②	Clayey silt	0.7~1.3	1710	6.9×10^{-7}	9.9×10^{-7}
③	Silty clay	0.8~2.1	1780	2.7×10^{-7}	5.1×10^{-7}
④	Muddy silty clay	3.4~5.4	1800	1.9×10^{-8}	3.7×10^{-7}
④$_{-1}$	Sandy silt	3.4~5.4	1840	7.2×10^{-7}	8.2×10^{-6}
⑤	Clay	3.3~4.6	1860	5.7×10^{-9}	7.5×10^{-9}
⑥	Sandy silt mixed with silty sand	15.3~17.0	1880	8.1×10^{-6}	2.5×10^{-5}
⑦	Silty clay	3.7~6.5	1920	6.8×10^{-8}	6.8×10^{-8}

Note: H – Thickness, ρ – Density, k_v – Vertical permeability coefficient, k_h – Horizontal permeability coefficient.

2.2.1. Water level monitoring system

At the construction site, 45 groundwater level observation wells and 2 artesian water level observation wells were strategically positioned around the foundation pit, with the locations indicated in Figure 3. Among them, SW3 and SW5 serve as artesian water level observation wells, while the others function as groundwater level observation wells. These observation wells are constructed using Φ 325×10 steel pipes with perforated walls, featuring 5mm diameter holes spaced at 50 mm intervals in a staggered pattern. They are wrapped in two layers of 40-mesh nylon mesh and an additional outer layer of 7-mesh wire mesh. The construction of these observation wells is synchronized with the excavation of the foundation pit, and water level data is systematically recorded. Water level measurements are conducted daily using a 30-meter steel ruler electronic water level measuring instrument as depicted in Figure 3. This instrument offers a minimum reading precision of 1.0 mm with a repeatable reading accuracy of 2.0 mm.

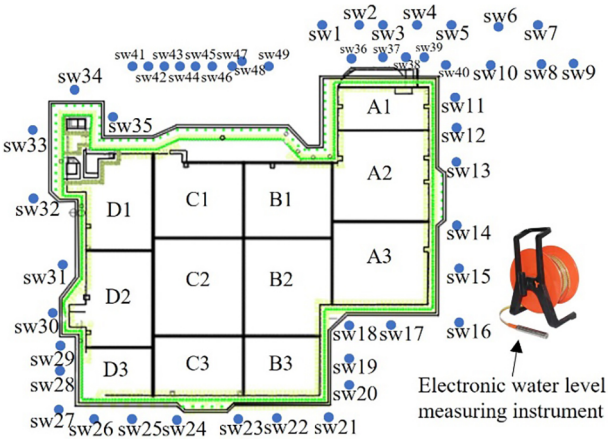

Figure 3. The layout plan of groundwater observation wells

2.2.2. Settlement observation system

The locations of these measurement points are illustrated in Figure 4. Around the foundation pit, a total of 18 ground settlement monitoring points, 11 railway subgrade settlement monitoring points, and 14 points along both sides of the high-speed railway subgrade were strategically positioned. The measurements were conducted using a Leica Total Station TS60, offering a measurement precision of 1 mm + 1 ppm. Observations were carried out daily, with a recording accuracy of 1mm. The ground settlement monitoring points were evenly distributed along the periphery of the foundation pit. Notably, DM1, DM17, and DM18 are located between the foundation pit and the railway, with DM1 falling within the subsequent in-situ dewatering test area, making it a focal point of observation. The railway subgrade displacement monitoring points are situated on the eastern side of the foundation pit, as well as the southeast side of the platform, with an approximate spacing of 15 meters between each point, designated as LJ1 to LJ11 for encoding. The high-speed railway subgrade measurement points were organized into 9 groups. Each odd-numbered group consisted of two measurement points, symmetrically positioned on both sides of the high-speed railway track axis. The even-numbered groups were placed on one side of the embankment, totaling 14 measurement points. The distance between each group of measurement points along the high-speed railway track was approximately 25 meters. A coding system, using GT1-1 to GT9-2, was employed for identification purposes.

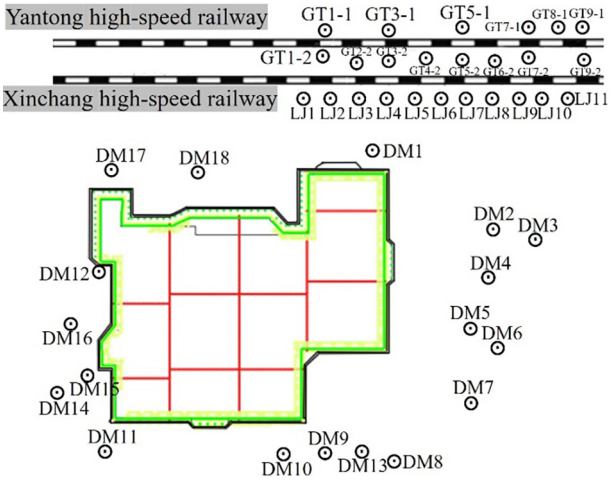

Figure 4. Distribution diagram of ground settlement measurement points

3. Analysis of the impact of excavation for the foundation pit on the surrounding environment

3.1. Construction scheme

The excavation of the foundation pit engineering project using a phased and layered open-cut method commenced on July 28, 2022. Reasonable zoning of the excavation can efficiently reduce the impact on the surrounding environment during the excavation process and minimize ground settlement outside the foundation pit (Li et al., 2017; Ding et al., 2018). The foundation pit was divided into 12 construction zones for sequential excavation, following the order of A1→A2→A3→B1→…→D2→D3, as illustrated in Figure 5. The excavation of the upper soil layers within the support system was completed by August 30, reaching a depth of approximately 4 meters. Subsequently, the excavation of the lower soil layers was completed by October 30, with a depth of approximately 6 meters. The bottom slab casting was finalized on November 30, marking the conclusion of the high-risk phase of the foundation pit excavation.

Groundwater level monitoring at the site commenced from the initiation of soil excavation. Due to site limitations, monitoring of surface subsidence around the foundation pit began at the end of August. At this point, the excavation of the upper soil layers within the support system had been completed, and monitoring of the displacement of the railway and high-speed railway subgrade began in mid-August. All monitoring data for various parameters

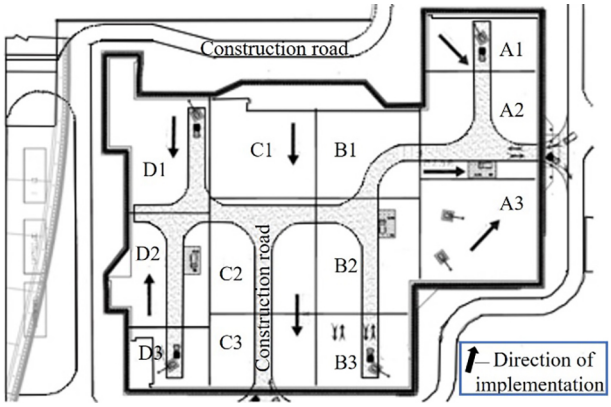

Figure 5. The schematic diagram of foundation pit zoning layout and construction direction

were recorded until January 3, 2023. At this time, both the upper and lower basements within the foundation pit had been entirely constructed, and the support system was gradually being dismantled following the construction sequence of the basement level, signifying that the impact of construction both inside and outside the pit had stabilized. In summary, the monitoring period effectively covered the high-risk construction phase, offering significant value for risk control and providing reference data for similar engineering projects.

3.2. Analyzing the impact of foundation pit excavation on groundwater

The on-site monitoring data substantiated the aforementioned deductions. Based on the excavation sequence of the foundation pit engineering, a statistical analysis was conducted on groups of observation wells located around specific blocks. These included SW11, SW37, and SW40 around the A1 block, SW43, SW45, and SW47 around the C1 block excavated during the intermediate stage, and SW25, SW26, and SW28 around the D3 block, which was excavated last. Due to minimal variation in observed water levels among adjacent phreatic layers, the average water levels of the surrounding phreatic layers for each block are considered as the water levels during excavation. The average water levels in the SW11, SW37, and SW40 phreatic layers are denoted as $\bar{A}1$. The average water levels in the SW43, SW45, and SW47 phreatic layers are denoted as $\bar{C}1$. The average water levels in the SW25, SW26, and SW28 phreatic layers are denoted as $\bar{D}3$.

During the construction phase, there exists an approximate 15-day interval between excavations in distinct construction blocks. Nevertheless, as illustrated in Figure 6, the fluctuations in water levels surrounding the construction blocks do not correspond to the excavation sequence. The temporal trends in groundwater level alterations across various sites exhibit similarity. This observation indicates that the isolative efficacy of the cutoff wall substantially mitigates the influence of foundation pit excavation on groundwater level variations beyond the pit to a negligible degree.

Among the observation wells, SW3 and SW5 serve as confined aquifer monitoring wells. Their water level changes in comparison to the adjacent phreatic layer observation wells are illustrated in Figures 7 and 8.

It is evident that the water levels in the confined aquifer and the phreatic layer exhibit a similar long-term trend.

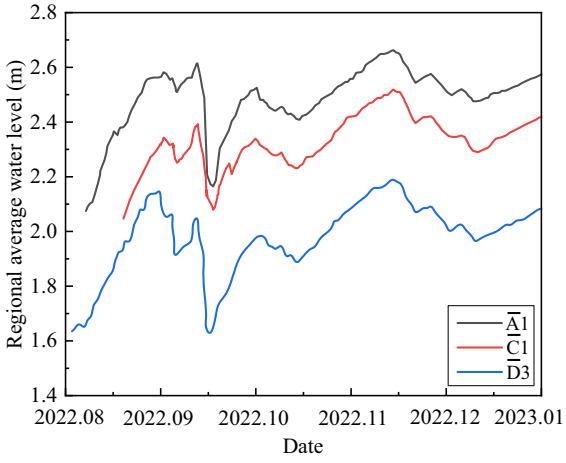

Figure 6. Schematic diagram of groundwater level changes around different construction areas

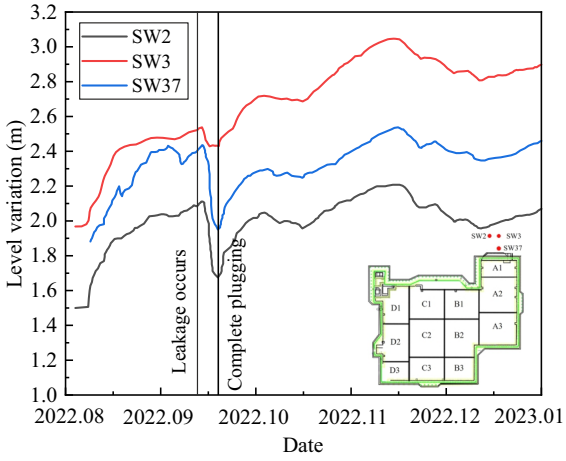

Figure 7. The level variation in SW3 pressurized well and surrounding submersible wells

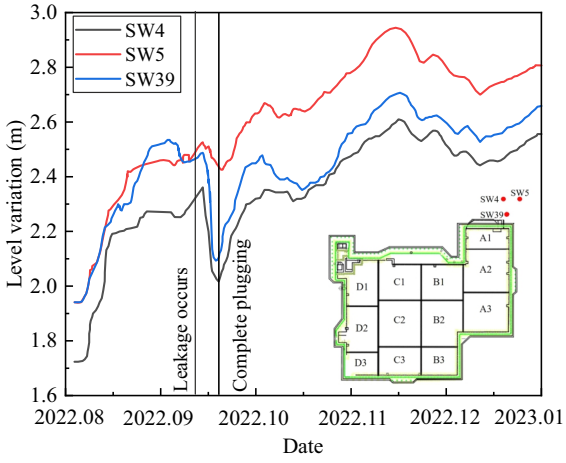

Figure 8. The level variation in SW5 pressurized well and surrounding submersible wells

However, when it comes to short-term water level fluctuations, the confined aquifer displays a more gradual response. For instance, considering the water level data for the week surrounding September 17th, from September 13th to September 15th, the local region encountered the effects of a typhoon along with precipitation, typically resulting in an anticipated elevation in groundwater levels. Nevertheless, owing to the partial detachment of the soil protection layer, as evidenced in the figure after heavy rainfall, localized seepage emerged along the inner wall of the pit support structure. After the typhoon's passage on the 15th and the cessation of precipitation, elevated temperature conditions ensued. Concurrently with seepage, the water level within the phreatic layer experienced a rapid decline. Throughout this timeframe, observation wells SW2 and SW37 within the phreatic layer manifested an average daily reduction in water level of 8.55 cm over five days spanning from September 13th to September 18th. In contrast, while confined aquifer observation well SW3 also witnessed a decrease in water level, its rate of decline amounted to 2.2 cm per day, approximately constituting 25.7% of the descent rate observed in the phreatic layer.

3.3. Analysis of the impact of foundation pit excavation on surface settlement

Statistical analysis was conducted on selected high-precision data points, namely DM1, DM2, DM3, DM14, and railway embankment monitoring point LJ3, which exhibited a linear increase in distance from the foundation pit, as depicted in Figure 4. The distances of these four monitoring points from the edge of the foundation pit are detailed in Table 2.

Table 2. Distance between monitoring points and foundation pit

Monitoring points	DM1	DM14	DM2	DM3	LJ3
Distance (m)	8.8	33.5	60.1	84.8	91.2

The subsidence variations at the aforementioned five monitoring points during the excavation period are depicted in Figure 9. The results indicate that significant settlement of the surrounding ground surface occurred during the foundation pit excavation phase. The most pronounced settlement was observed at point DM1, located within a distance of one excavation depth. As the distance between the monitoring points and the foundation pit increased, the settlement values gradually diminished. Following the casting of the foundation pit's bottom slab, apart from the DM1 point closest to the pit's edge, the settlement values at the remaining monitoring points essentially stabilized.

By the end of the monitoring period, the subsidence at the DM1 point, which is closest to the foundation pit, was approximately 8.63 mm, while DM14 experienced approximately 5.54 mm of subsidence. DM2 and DM3 recorded subsidence of around 4.21 mm and 2.19 mm, respectively.

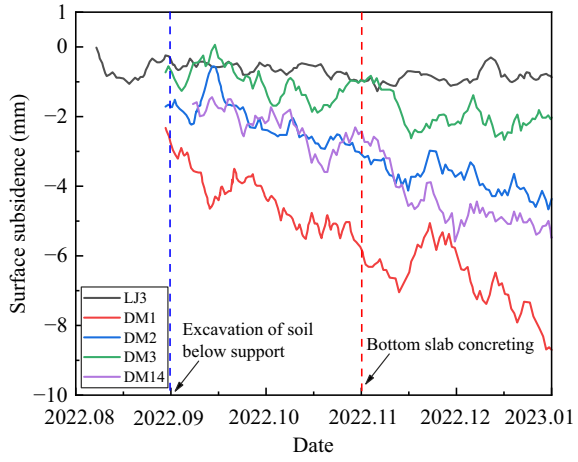

Figure 9. The settlement changes at each monitoring point

In contrast, the farthest railway monitoring point, TL3, exhibited subsidence that did not exceed 1 mm throughout the observation period. Despite TL3's proximity to DM3 regarding the distance from the foundation pit's edge, its subsidence was only half of that observed at DM3. Additionally, the fluctuations in TL3's subsidence during the monitoring period were less pronounced compared to DM3. This discrepancy may be attributed to the reinforcing effect of the railway subgrade on TL3. Furthermore, it could also be influenced by the diverse and irregular factors affecting DM3, such as material stacking and irregular vehicle loading, as DM3 was situated within the construction zone. The railway department stipulates that the allowable value of track settlement is 3–5 mm, with 3 mm for initial settlement and 5 mm for long-term settlement. Statistical analysis of monitoring point LJ3 on the railway embankment shows that the fluctuation value of railway embankment settlement during construction is less than 2.0 mm. During the construction of this foundation pit, it meets the standard for high-speed railway foundation settlement and does not affect the normal operation of the railway.

The overall trend in subsidence for the closely located DM1, DM2, and DM3 monitoring points remained consistent, with a brief deviation observed around September 15th. This deviation may be attributed to the storm surge mentioned earlier, which resulted in seepage along the inner wall of the foundation pit near the DM1 monitoring point. During this period, while DM2 and DM3 monitoring points exhibited uplift due to the elevated groundwater level in the phreatic layer, DM1 experienced accelerated subsidence. This was primarily due to the combined effects of stress release caused by the excavation of the foundation pit and the lowering of the groundwater table. Subsequently, DM1 briefly rebounded after the implementation of improved dewatering and sealing measures. Following this rebound, all monitoring points generally continued to subside, with localized rebounds possibly associated with increased groundwater levels during continuous rainfall. However, throughout the water level maintenance period, the surface behavior remained predominantly character-

ized by subsidence induced by the excavation of the foundation pit. Figure 9 shows that monitoring points DM1, DM2, and DM14 around the pit continue to sink even after the bottom slab concreting. Even after construction is completed, some monitoring points may still show a certain degree of settlement due to uneven settlement of the foundation or the nature of the foundation materials. In addition, changes in groundwater levels, construction quality of the foundation engineering, and surrounding environmental factors may also affect the settlement of monitoring points.

3.4. Simulation analysis of foundation pit excavation

The 3D model of foundation pit excavation and support during the construction process was established based on Section 3.1, and simulation calculations were conducted on the surface settlement during the excavation and support process of the foundation pit. According to on-site monitoring data, the influence radius of the foundation pit is less than 100 m, and the model size is selected as 362 m × 322 m × 60 m, as shown in Figure 10. The model calculation adopts a coupled numerical method, with the constitutive model selected as Mohr-Coulomb and the seepage model selected as isotropic. The fluid-mechanical coupling effect is considered using the Biot consolidation theory. The lateral boundary of the model is supplied with a constant head, with no cross-flow replenishment in the confined aquifer. The model's lateral boundaries are fixed with the "fix" command to maintain a constant head, with the top and bottom plates of the confined aquifer set as impermeable materials. There is no cross-flow replenishment between soil layers, and the water-resisting curtain is made of impermeable material, which acts as a barrier to hydraulic connection inside and outside the foundation pit.

Figure 11 shows the vertical deformation profile of the soil layers. The measured data and simulated data (S-LJ3 and S-DM1) of key points LJ3 near the settlement monitoring rail and the closest point DM1 to the foundation pit are compared as shown in Figure 12. The numerical simulation ground settlement values are basically consistent with the actual monitoring values. The actual monitoring values fluctuate due to significant external environmental influences such as construction vibration and temperature. However, the simulation results can provide a reliable reference for foundation pit settlement monitoring and also serve as a reliable basis for excavation schemes of the foundation pit.

4. The recharging tests and result analysis

4.1. Experimental design

The present experiment was well-suited for constant-head injection tests and falling-head injection tests within confined aquifers, as well as constant-head injection tests and falling-head injection tests within the phreatic layer.

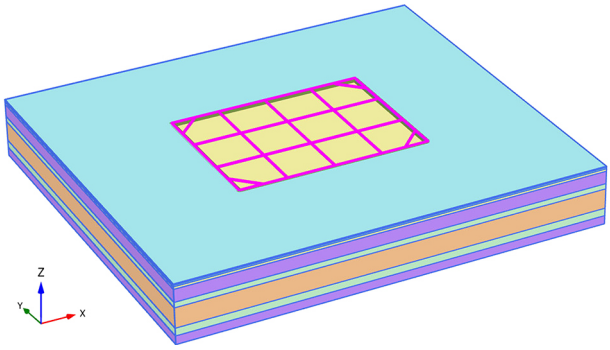

Figure 10. 3D numerical model

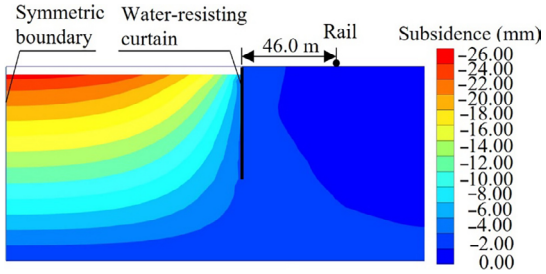

Figure 11. Profile cloud map of soil deformation

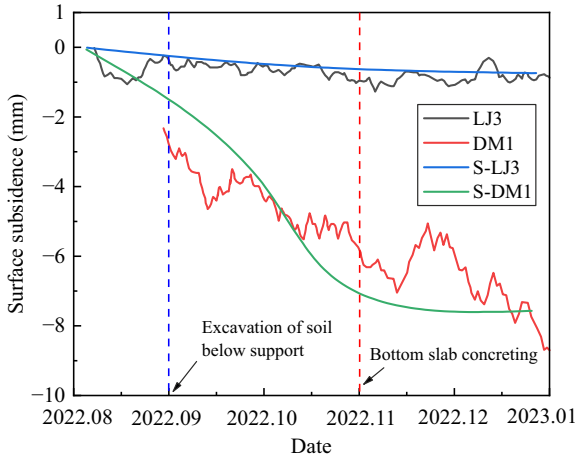

Figure 12. Comparison chart of measured curves and simulated curves for LJ3 and DM1

Consequently, the experiment comprised four groups: confined aquifer variable-head recharge tests, confined aquifer constant-head recharge tests, phreatic layer falling-head recharge tests, and phreatic layer constant-head recharge tests.

In the falling head water recharge test, the procedure begins with the initial recording of the original water level H_i in the recharge well. Subsequently, the water level in the recharge well is rapidly raised to a specified elevation, recorded as the initial water level H_0. The water supply is then immediately halted, and this moment is documented as the initial time t_0. An electronic level gauge is employed to record the subsequent variations in the water level within the recharge well, with the water level at time "t" denoted as H_t. This process continues until the water level within the recharge well has returned to its

original level. A semi-logarithmic plot is used to depict the relationship between the water head decline and time. A linear trend on the graph indicates the accuracy of the results. Concurrently, monitoring of water level changes in the two nearest observation wells around the recharge well is maintained for comparative purposes.

In the constant head water recharge test, the procedure initiates with the recording of the initial water level H_i within the recharge well. Subsequently, the recharge valve is opened, rapidly raising the water level in the recharge well to a specified elevation, which is documented as the initial water level H_0. The moment this is achieved is designated as the initial time t_0. Following this, the inflow rate is gradually reduced to maintain the water level in the recharge well at H_0. Flow measurements are taken at 5-minute intervals for the first five measurements and at 20-minute intervals thereafter. This continues until the water level in the observation well stabilizes and remains unchanged for 60 minutes. When the consecutive flow measurements exhibit a difference of no more than 10%, the mean of the stable injection rates is calculated as the injection rate for further analysis.

4.2. Calculation methods for permeability coefficient

In the constant head water recharging test, a continuous flow of water is introduced into the borehole to maintain a constant water level. The permeability coefficient K of the lower section of the borehole can be expressed using the equation presented in Eqn (1):

$$K = \alpha \frac{q}{\pi d \Delta h} = \frac{q}{A \Delta h}, \tag{1}$$

where q is the stable water recharging rate; d is the diameter of the hole; Δh is the stable head difference formed in the hole; α is the correction coefficient based on the inflow situation and seepage path; and A is the shape factor.

In the drilling dewatering head recharging test, in accordance with Darcy's law, within a given small time period, as follows:

$$qdt = K \frac{H}{l} M dt, \tag{2}$$

where q is the stable water recharging rate; K is the permeability coefficient; H is the head difference inside the hole; l is the length of the seepage path; M is the penetration section area.

Assuming the inner diameter area of the well is represented as "a", Eqn (2) can be expressed as:

$$K \frac{H}{l} M dt = a dH. \tag{3}$$

Integrating between t_1 and t_2 at any time, the corresponding water head decreases from H_1 to H_2, resulting in:

$$K \frac{M}{l} \int_{t_1}^{t_2} dt = a \int_{H_1}^{H_2} \frac{dH}{H}; \tag{4}$$

$$K = \frac{al}{M} \frac{\ln \frac{H_1}{H_2}}{t_2 - t_1} = \frac{\pi d}{4A} \frac{\ln \frac{H_1}{H_2}}{t_2 - t_1} = \frac{\pi r^2}{A} \frac{\ln \frac{H_1}{H_2}}{t_2 - t_1}, \tag{5}$$

where A is the shape factor. The test section is situated below the groundwater level. If water infiltrates the bottom of the hole, then $A = 5.5r$. If water infiltrates the bottom of the hole, and the top plate of the test soil layer is impermeable, then $A = 4r$.

The method described above necessitates the complete restoration of the water level in the recharge well to its original state. Alternatively, there is also a characteristic time method that allows for a swift calculation of the permeability coefficient of low-permeability soil layers. This method is based on the linear relationship between the head drop ratio and time, represented on a semi-logarithmic scale:

$$K = \frac{\pi r^2}{A T_0}, \tag{6}$$

where T_0 is the characteristic time of the water recharging process and the time corresponding to $H_t/H_0 = 0.37$ is considered as the characteristic time.

4.3. Monitoring results of the recharging tests

SW3 observation well was selected as the recharge well, with a depth of 15.1 meters. The well's bottom screen was positioned within the 5th confined aquifer layer. The original water level was 279.0 cm below the wellhead. Subsequently, the water level was rapidly recharged to an initial position of 118.0 cm below the wellhead. After 380 minutes, the water level decreased to a position 278.0 cm below the wellhead. Assuming the original hydraulic head as H_i = 0.0 cm, the initial recharge water level is calculated as H_0 = 279.0 cm − 118 cm = 161.0 cm. The variations in water level inside the well H_t were then recorded, and the relationship between confined aquifer hydraulic head decline and time was plotted on a semi-logarithmic coordinate axis, as shown in Figure 13a.

As shown in Figure 13a on a semi-logarithmic coordinate axis, the curve exhibits a linear shape, indicating that the experimental process largely conforms to Darcy's flow law. Utilizing this method allows for an effective determination of its osmosis coefficient. By selecting data from a linear segment with minimal error, and applying it to the theoretical calculation section of the borehole falling head water recharging test theory in Section 4.2, the confined aquifer's osmosis coefficient is calculated to be 1.954×10^{-3} cm/s. Furthermore, by reading T_0 as 104 minutes on the semi-logarithmic coordinate axis and employing the characteristic time calculation method, the osmosis coefficient is determined to be 2.012×10^{-3} cm/s.

Utilizing the same methodology, we can determine the permeability coefficients for W1, SW2, SW4, and SW5. The comparison between the calculated results and the permeability coefficients from the geological exploration report is presented in Table 3.

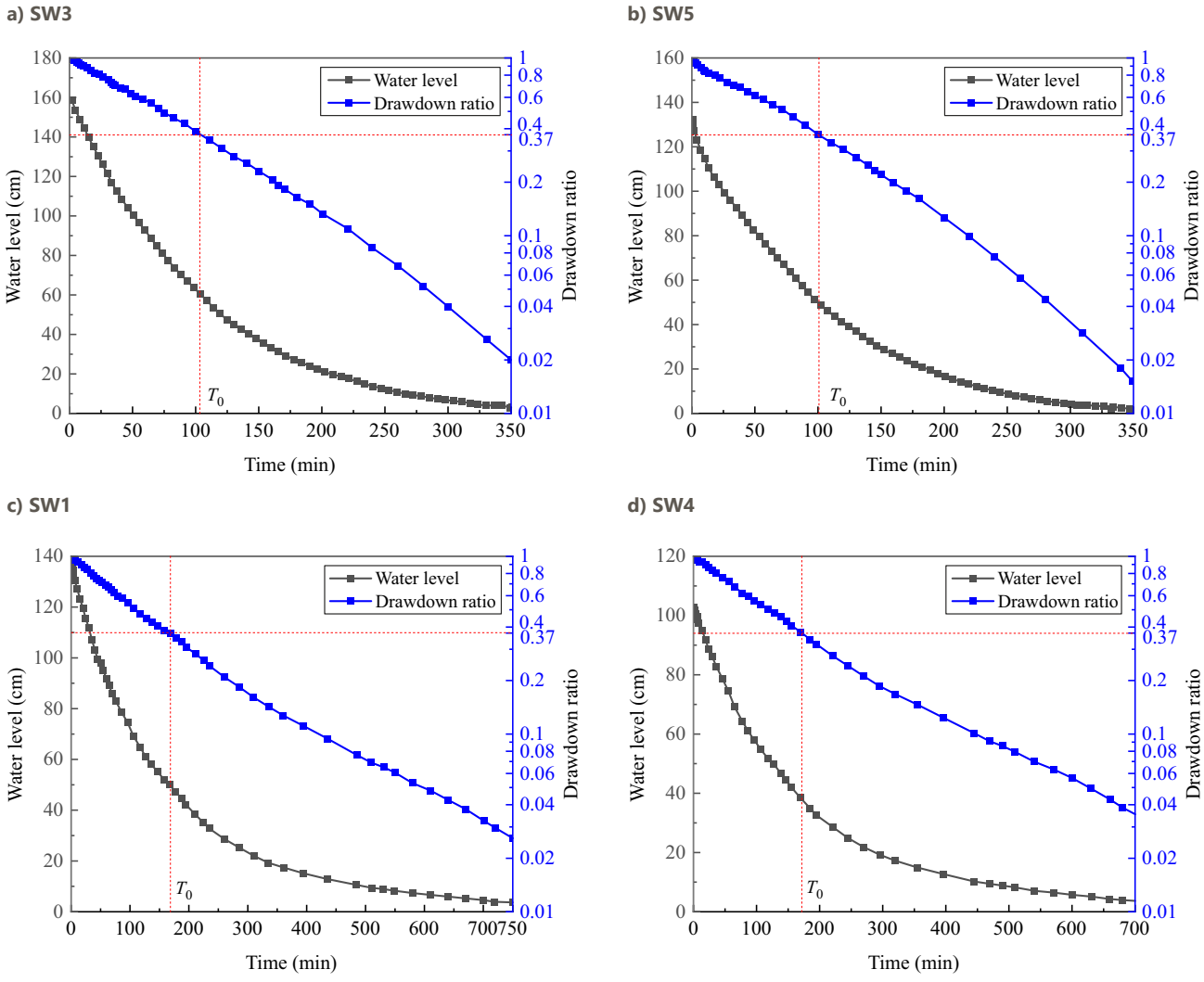

Figure 13. The water level variation diagram of precipitation head recharge tests

Table 3. Comparison of permeability coefficients obtained by different calculation methods

Layer	Geological survey report		Precipitation head test Theoretical		Characteristic time method Calculated value		Constant head test Theoretical
④$_{-1}$	k_v	k_h	SW1	SW4	SW1	SW4	SW2
	7.2×10^{-7}	8.2×10^{-6}	8.1×10^{-6}	8.2×10^{-6}	9.0×10^{-6}	8.8×10^{-6}	8.8×10^{-6}
⑥	k_v	k_h	SW3	SW5	SW3	SW5	SW5
	8.1×10^{-6}	2.5×10^{-5}	2.0×10^{-5}	2.0×10^{-5}	2.012×10^{-5}	2.1×10^{-5}	2.1×10^{-5}

4.4. Data analysis and discussion

It is evident that, for the confined aquifer, the calculated permeability coefficients fall within the range between the vertical and horizontal coefficients presented in the geological report. This suggests that the in-situ water recharge test provides an effective and reasonably accurate means to assess the permeability of well-behaved soil. For the phreatic layer, most of the calculated results exceed the horizontal permeability coefficients, which are higher than other values from the geological report. This discrepancy may be attributed to the fact that the geological report results are averaged from multiple boreholes and soil samples, with differences in permeability coefficients within each borehole potentially exceeding fourfold, or even an order of magnitude. This variance indicates significant variability in permeability within the same soil layer. The chosen well locations for the phreatic layer test happened to be in areas with higher permeability. Additionally, it's worth noting that when the soil's permeability is lower, determining the precise time corresponding to a particular water level can be more challenging due to the slower rate of water level decline. This challenge can introduce greater calculation errors. In summary, when conducting in-situ water recharge tests to determine the permeability of well-behaved soils, results can be considered scientifically valid

and valuable for reference when they are within the same order of magnitude as those in geological reports. However, it's essential to recognize that in-situ water recharge tests are more suitable for soil layers with better permeability, where the results are more accurate.

The experimentally determined osmosis coefficients are notably closer to the permeability in the horizontal direction, which exhibits higher permeability compared to other orientations. This observation could be attributed to the distinct conditions during the in-situ water recharge test compared to laboratory bench-scale experiments. In the field, below the bottom of the recharge well, the pressure from the recharge head expedites the rapid lateral spreading of water in the well along the direction of higher horizontal permeability coefficients in the surrounding area.

The utilization of the characteristic time method offers the advantage of a straightforward formula and shorter testing durations. Given the trade-off between the time required for the test and the level of precision achieved, it can be concluded that, for most engineering applications, employing the characteristic time method is both reasonably accurate and resource-efficient for the determination of well-point osmosis coefficients.

The osmosis coefficients obtained using the constant head method tend to be relatively higher, possibly due to prolonged high hydraulic head conditions leading to the establishment of more permeable flow paths within the soil. While the in-situ recharge method may not distinctly differentiate between the vertical and horizontal permeability characteristics of the soil, it is the most effective approach in reflecting the practical water recharge process. It aligns well with the actual recharge capabilities of well points based on construction and site-specific conditions, particularly in the case of constant head recharge. Consequently, the well recharge capacity determined through constant head tests holds significant practical value for specific engineering applications.

5. Numerical simulation analysis

5.1. Model establishment and calculation results

In this model, simulations were conducted using the porous media elasticity model and the modified Cambridge model. The recharge well had a depth of 10 meters with a 1-meter distance from the bottom to the phreatic layer, allowing only the bottom of the well to be permeable. On the left side of the model, there was an impermeable boundary representing the function of a water-resisting curtain, which, based on the actual layout in the foundation pit engineering site in Yancheng, was positioned at a distance of 15 meters from the recharge well. On the right side, a fixed pressure boundary was set at a distance of 100 meters from the recharge well to simulate lateral hydraulic recharge from the surrounding geological formation. The model parameters are detailed in Table 4, and the calculation model is illustrated in Figure 14.

The numerical calculations were conducted in the following steps:

- Step 1: Initial geo-stress equilibrium was established.
- Step 2: Excavation of the upper part of the recharge well was simulated, with horizontal displacement of the wellbore constrained.
- Step 3: Excavation of the lower part of the recharge well was simulated, with horizontal displacement of the wellbore constrained.
- Step 4: A pore pressure of 86.2 kPa was applied at the bottom of the well, simulating a constant recharge water level of 1.6 meters. Transient calculations were performed with time steps not exceeding 1800 seconds, simulating 10 days of recharge.
- Step 5: Maintaining constant recharge pressure, transient calculations continued with time steps not exceeding 86400 seconds, simulating 150 days of recharge.
- Step 6: With the recharge pressure held constant, steady-state calculations were performed to assess the final impact of the recharge.

The seepage vector diagrams at 10 minutes, 12 hours, 50 days, and 160 days after the commencement of recharge are depicted in Figure 15. During the early stages of recharge, water from the recharge well spreads outward from the bottom of the well as a high-pressure center. Both the pore pressure contour plots and the flow vector maps exhibit a roughly symmetric distribution around the

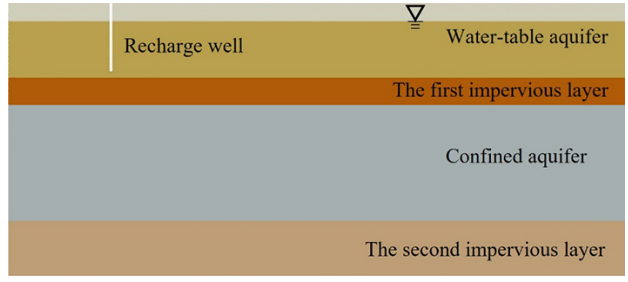

Figure 14. The calculation model for groundwater recharge outside the water stop curtain

Table 4. Model material elastic-plastic material parameters

Layer	Permeability	Resilience index κ	Compressive index λ	Mritical stress ratio *M*
①	Water-table aquifer	0.063	0.139	0.25
②	First impervious layer	0.022	0.048	0.33
③	Load-bearing aquifer	0.011	0.052	0.98
④	Second impervious layer	0.020	0.045	0.33

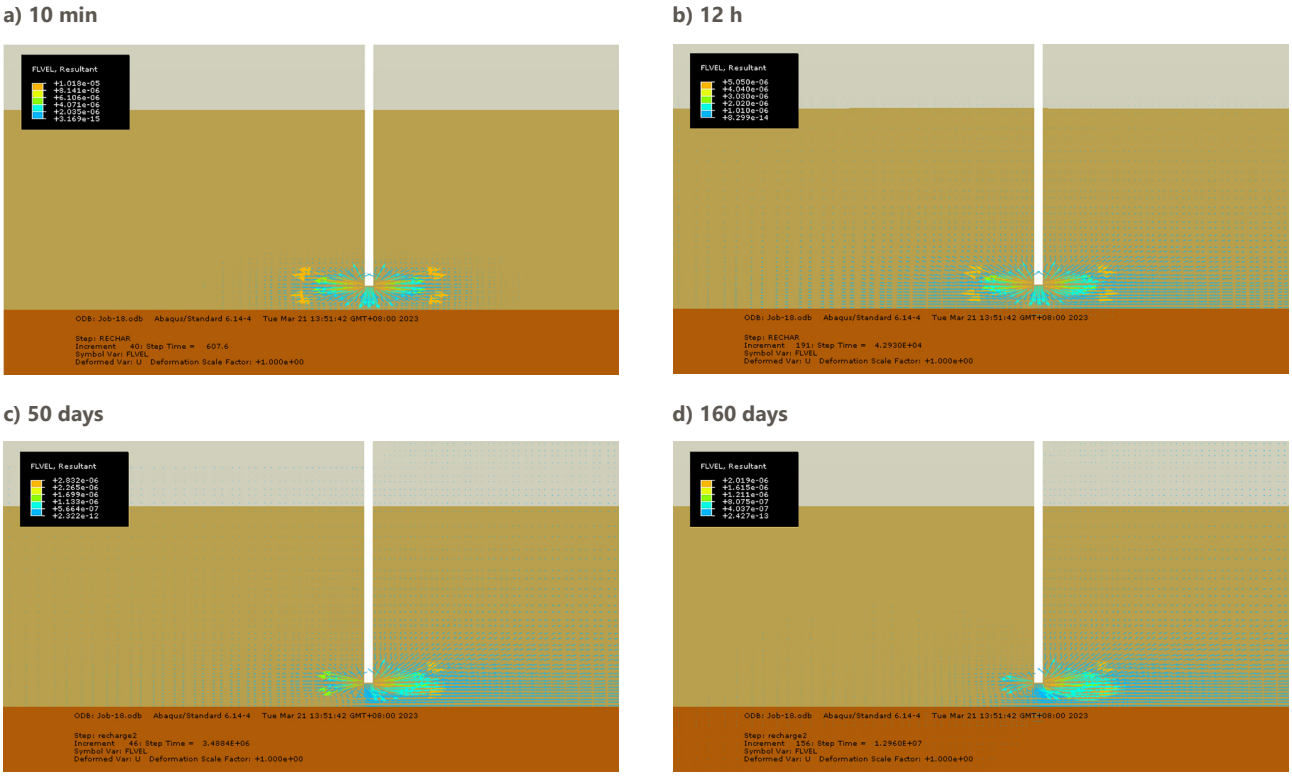

Figure 15. The seepage vector diagrams during recharging

recharge well, with primary recharge flow occurring within the phreatic layer. The first aquitard layer demonstrates an effective confining influence. Approximately one day after the onset of recharge, differences in flow become noticeable on both sides of the recharge well. After around 160 days of recharge, a stable state is reached.

5.2. The impact of recharge on groundwater

The direct impact of water recharge on the soil is the alteration of its pore water pressure. Variations in pore pressure subsequently result in changes in the stress state within the soil and ultimately lead to surface settlement alterations. Initially, the focus is on examining the pore pressure changes along different depth levels within horizontal cross-sections induced by the recharge process. Three sections are selected for observation: one at the phreatic layer bottom (–11 m) and two others at depths of –7 m and –3.8 m below the ground surface. Figure 16 presents the pore pressure values at these three sections after the completion of the water recharge.

As shown in Figure 16, the pore pressure variations exhibit a consistent trend at different depths. However, the pore pressure difference between the two sides of the water recharge well tends to decrease as the depth increases. At –3.8 m depth, the difference is 5.3 kPa, while at –7 m, it is 4.4 kPa. At the bottom of the phreatic layer, the same difference at the corresponding location is merely 0.1 kPa. Vertical pore pressure profiles are depicted in Figure 17 at three positions: 0.8 m on both sides of the water recharge well (L1, R1) and 40 m away from the water-resisting curtain (R2). Below the first impervious layer, these profiles exhibit identical pore pressures, indicating that the confined aquifer remains unaffected by the aquifer replenishment mainly due to the presence of the impermeable layer.

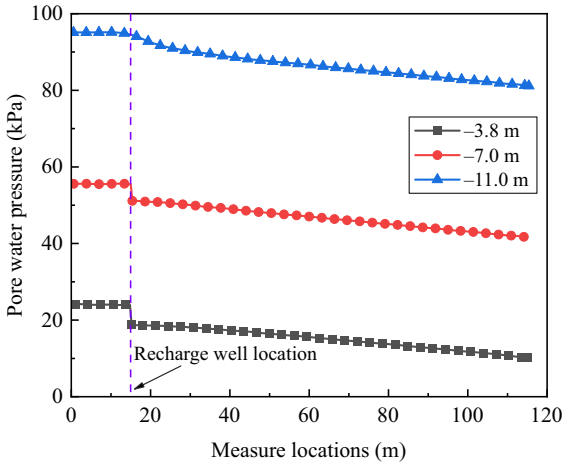

Figure 16. Variation of pore water pressure at different depths

Figure 17 provides an enlarged view of the pore pressure change curve. It is evident that the pore pressure values along the L1 and R1 profiles are identical, which are located equidistant from the center of water recharge at the bottom of the phreatic layer. In the phreatic layer, the pore pressure variations with depth exhibit slopes that closely resemble the gravitational gradient, particularly between the L1 and R2 sections. Meanwhile, the slope of L1

is initially steeper and then gradually tapers off. These observations suggest the establishment of a "water storage effect" between the recharge well and the water-resisting curtain, where the seepage activity within this "reservoir" remains relatively stable. The recharge creates a head differential on either side of the well, leading to horizontal seepage outside the recharge well, resulting in relatively unstable pore pressure distribution over short distances on the outer side of the well.

5.3. The impact of recharge on ground heave

Under the influence of recharge, the surface undergoes uplift due to changes in pore pressure that, in turn, lead to alterations in the stress state within the soil. Figure 18 presents the final distribution of vertical uplift. It is evident that, with a recharge in effect, uplift occurs uniformly around the recharge well. This uplift primarily arises from the cumulative uplift of the soil within the phreatic layer above the plane of the well bottom. The impervious layer and the underlying strata essentially remain unaltered, making no significant contribution to ground heave. As mentioned in Section 5.2, pore pressure beneath the impervious layer shows no variation, confirming that uplift results from pore pressure changes within the soil. Table 5 provides details of the characteristics of the five marked observation points (#1~#5) in Figure 18, along with their respective distances from the center of the recharge well.

Figure 19 illustrates the temporal variation of ground heaves at five observation points during the recharge process. It is evident that all surface points exhibit uplift under the influence of recharge, with consistent trends observed on both sides of the recharge well. Uplift occurs more rapidly on the side closer to the water-resisting curtain, and it reaches the stable uplift value earlier. Additionally, proximity to the recharge well results in higher uplift values. However, the final ground heave values become largely uniform once the seepage stabilizes.

The ground heave can be distinctly divided into two phases, with the first phase occurring within the initial two days, as summarized in Table 6. During this first phase, the ground heave increases rapidly, with all observation points, except for point 5, reaching over 30% of their final stable uplift within the initial two days. This indicates that within the first 1.25% of the recharge duration, the ground heave had already reached 30% of its final value. Point 5, being the farthest from the recharge center, required a longer time to fully manifest the effects of recharge. Nevertheless, it still exhibited an uplift of 16.8% during the first phase, notably higher than in the second phase. These results underscore the importance of distinguishing between various objectives when implementing recharge methods for ground settlement control in practical engineering. Depending on the specific goals, different recharge amounts, and durations should be considered within the recharge strategy, such as for emergency settlement control versus long-term settlement control.

Figure 20 shows the surface uplift variation at point 2 along with the groundwater level variation and pore pressure changes at depths of 3.7 m, 5.5 m, and 9 m beneath. It is evident that the vertical surface uplift correlates closely with groundwater fluctuations. Aligning the curves at both ends to observe the temporal trends of the parameters reveals that during the early stages of recharge, the surface uplift rate is significantly higher than the groundwater level recovery rate. Moreover, closer to the well bottom, pore pressure changes exhibit greater rate and magnitude variations compared to surface subsidence. At a depth of 9 m, this influence is especially pronounced. Thus, a much more rapid response of pore pressure changes compared to surface subsidence. This evolution from shallow to deep leads to a linear relationship between pore pressure variations at a certain depth and surface uplift values over the entire recharge process. In this example, the surface uplift curve closely matches the 5.5 m pore pressure variation curve, allowing for linear inference of surface uplift based on pore pressure changes. Groundwater level changes, on the other hand, exhibit lag due to the time required for groundwater to flow through the subsurface. Consequently, their changes are relatively gentle during the early stages of recharge and do not promptly reflect surface uplift. Pore pressure changes, occurring instantaneously with stress alterations, induce soil deformation and surface uplift.

Table 5. Observation points selection feature table

	Characteristic	Distance from recharge well
#1	Near the starting point of the largest uplift on the side of the foundation pit	3.5 m
#2	Recharge well and curtain midpoint	7.8 m
#3	The maximum uplift starting point far from the foundation pit side	2.2 m
#4	#4 is the symmetrical point along the reinjection well for # 2	7.8 m
#5	Stay away from the reference point of the recharge well	30.0 m

Table 6. Proportion of first stage uplift at each observation point

	Time (day)	#1	#2	#3	#4	#5
First phase	2	11.48 mm	11.10 mm	8.07 mm	7.25 mm	2.31 mm
Final stage	160	36.74 mm	36.64 mm	20.14 mm	19.55 mm	13.72 mm
Proportion	1.25%	31.2%	30.3%	40.1%	37.1%	16.8%

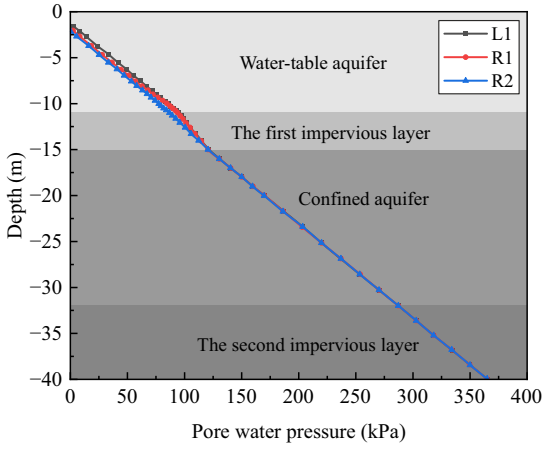

Figure 17. Vertical profile pore pressure variation

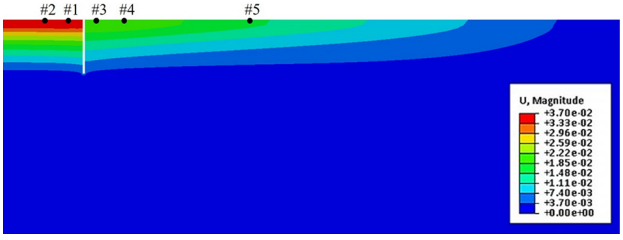

Figure 18. The cloud map of soil uplift distribution after recharge

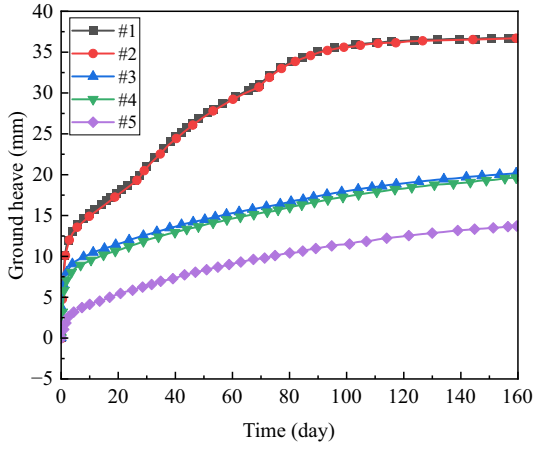

Figure 19. The observation points surface uplift changes over time

Thus, groundwater level changes lag behind deep pore pressure variations. This indicates that when employing phreatic layer recharge, the surface uplift closely relates to the pore pressure values within the stable deep flow region of the phreatic layer. In regions with lower precision requirements, one can estimate recharge effects based on groundwater level changes within this stable flow area.

6. Conclusions

This study is based on the foundation pit excavation project of a comprehensive high-speed rail station hub construction. It investigates the groundwater flow and soil settlement behavior under the influence of dewatering

a) Relationship between the ground heave and groundwater level

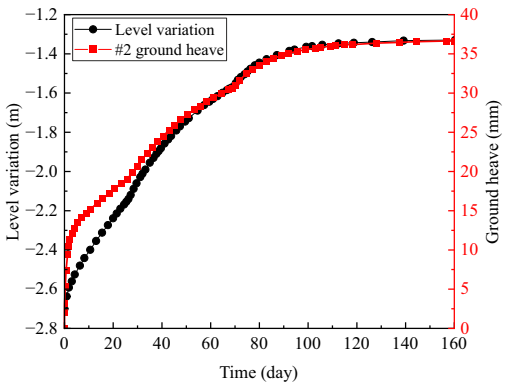

b) Relationship between the ground heave and the pore water pressure at 3.7 m

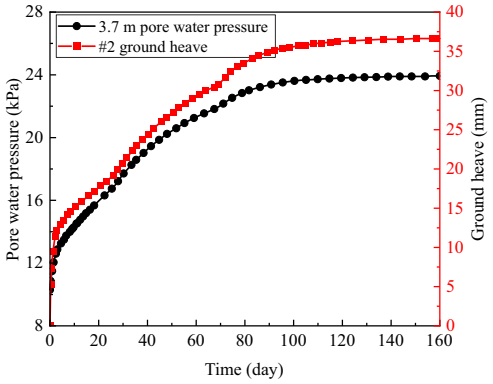

c) Relationship between the ground heave and the pore water pressure at 5.5 m

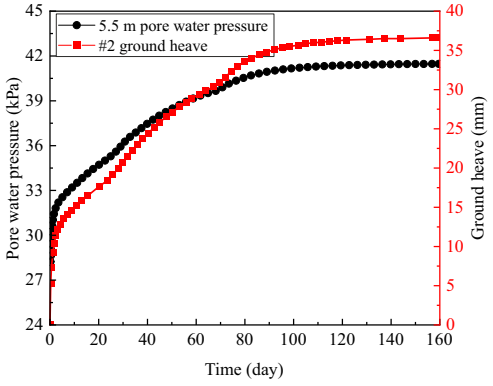

d) Relationship between the ground heave and the pore water pressure at 9.0 m

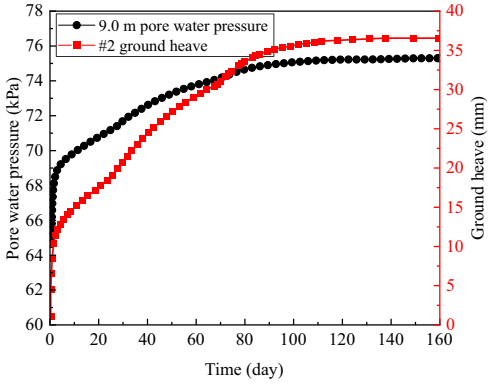

Figure 20. Relationship between the ground heave and groundwater and the pore water pressure

and water recharge during the foundation pit excavation. The investigation combines on-site monitoring, recharge tests, and numerical simulations. The primary conclusions are as follows:

(1) During the foundation pit excavation, the water-resisting curtain effectively mitigated the impact on the surrounding groundwater levels. The confined aquifer and phreatic layer exhibited distinct variations in groundwater levels, with the curtain significantly reducing fluctuations. The fluctuation value of railway embankment settlement is less than 2.0 mm, meeting the standard for high-speed railway foundation settlement.

(2) The results of the confined aquifer tests are consistent with the permeability coefficient in the geological survey report, and the recharging tests exhibit higher accuracy in soil layers with good permeability. Below the bottom of the injection well, under the pressure of the injection head, water in the injection well can rapidly spread horizontally around it along directions with higher permeability coefficients, leading to an overestimation of horizontal permeability coefficients in the aquifer test results.

(3) During the recharging process, the pore pressure in the aquifer is sensitive to recharging, and impermeable layers restrict seepage, leading to differences in pore pressure. Surface uplift is mainly influenced by the uplift of the aquifer soil, with the maximum uplift occurring near the recharging wells. Groundwater level changes lag behind pore pressure, and surface uplift during aquifer recharging can be estimated through pore pressure data. Proper recharging can effectively prevent ground settlement during the excavation of the foundation pit.

References

Chen, R., Meng, F., Li, Z., Ye, Y., & Ye, J. (2016). Investigation of response of metro tunnels due to adjacent large excavation and protective measures in soft soils. *Tunnelling and Underground Space Technology*, *58*, 224–235. https://doi.org/10.1016/j.tust.2016.06.002

Chen, S., Cui, J., & Liang, F. (2022). Case study on the deformation coupling effect of a deep foundation pit group in a coastal soft soil area. *Applied Sciences*, *12*(12), Article 6205. https://doi.org/10.3390/app12126205

Ding, Z., Jin, J., & Han, T.-C. (2018). Analysis of the zoning excavation monitoring data of a narrow and deep foundation pit in a soft soil area. *Journal of Geophysics and Engineering*, *15*(4), 1231–1241. https://doi.org/10.1088/1742-2140/aaadd2

Dong, Y., Burd, H., Houlsby, G., & Hou, Y. (2014). Advanced finite element analysis of a complex deep excavation case history in Shanghai. *Frontiers of Structural and Civil Engineering*, *8*(1), 93–100. https://doi.org/10.1007/s11709-014-0232-3

Faheem, H., Cai, F., & Ugai, K. (2004). Three-dimensional base stability of rectangular excavations in soft soils using FEM. *Computers and Geotechnics*, *31*(2), 67–74. https://doi.org/10.1016/j.compgeo.2004.02.005

Finno, R. J., Blackburn, J. T., & Roboski, J. F. (2007). Three-dimensional effects for supported excavations in clay. *Journal of Geotechnical and Geoenvironmental Engineering*, *133*(1), 30–36. https://doi.org/10.1061/(ASCE)1090-0241(2007)133:1(30)

Finno, R. J., & Roboski, J. F. (2005). Three-dimensional responses of a tied-back excavation through clay. *Journal of Geotechnical and Geoenvironmental Engineering*, *131*(3), 273–282. https://doi.org/10.1061/(ASCE)1090-0241(2005)131:3(273)

Guo, F., Wang, G.-H., & Li, Z.-C. (2022). Influence of artificial recharge in a phreatic aquifer on deep excavation dewatering: A case study of Dongguantou Nan Station in Beijing, China. *Hydrogeology Journal*, *30*(2), 673–689. https://doi.org/10.1007/s10040-021-02441-w

Hou, Y. M., Wang, J. H., & Zhang, L. L. (2008). Finite-element modeling of a complex deep excavation in Shanghai. *Acta Geotechnica*, *4*(1), 7–16. https://doi.org/10.1007/s11440-008-0062-3

Jan, J. C., Hung, S. L., Chi, S. Y., & Chern, J. C. (2002). Neural network forecast model in deep excavation. *Journal of Computing in Civil Engineering*, *16*(1), 59–65. https://doi.org/10.1061/(ASCE)0887-3801(2002)16:1(59)

Li, M.-G., Zhang, Z.-J., Chen, J.-J., Wang, J.-H., & Xu, A.-J. (2017). Zoned and staged construction of an underground complex in Shanghai soft clay. *Tunnelling and Underground Space Technology*, *67*, 187–200. https://doi.org/10.1016/j.tust.2017.04.016

Liao, S.-M., Wei, S.-F., & Shen, S.-L. (2016). Structural responses of existing metro stations to adjacent deep excavations in Suzhou, China. *Journal of Performance of Constructed Facilities*, *30*(4), Article 04015089. https://doi.org/10.1061/(ASCE)CF.1943-5509.0000845

Liu, H., Li, P., & Liu, J. (2011). Numerical investigation of underlying tunnel heave during a new tunnel construction. *Tunnelling and Underground Space Technology*, *26*(2), 276–283. https://doi.org/10.1016/j.tust.2010.10.002

Mohammadzadeh-Habili, J., & Khalili, D. (2020). Assessment of artificial recharge dams and improvement of their groundwater-recharge capacity. *Journal of Hydrologic Engineering*, *25*(5), Article 04020011. https://doi.org/10.1061/(ASCE)HE.1943-5584.0001909

Roy, D., & Robinson, K. E. (2009). Surface settlements at a soft soil site due to bedrock dewatering. *Engineering Geology*, *107*(3–4), 109–117. https://doi.org/10.1016/j.enggeo.2009.05.006

Schäfer, R., & Triantafyllidis, T. (2006). The influence of the construction process on the deformation behaviour of diaphragm walls in soft clayey ground. *International Journal for Numerical and Analytical Methods in Geomechanics*, *30*(7), 563–576. https://doi.org/10.1002/nag.480

Son, M., & Cording, E. J. (2008). Numerical model tests of building response to excavation-induced ground movements. *Canadian Geotechnical Journal*, *45*(11), 1611–1621. https://doi.org/10.1139/t08-074

Song, D., Chen, Z., Dong, L., Tang, G., Zhang, K., & Wang, H. (2020). Monitoring analysis of influence of extra-large complex deep foundation pit on adjacent environment: a case study of Zhengzhou City, China. *Geomatics, Natural Hazards and Risk*, *11*(1), 2036–2057. https://doi.org/10.1080/19475705.2020.1823492

Sun, Y., & Xiao, H. (2021). Wall displacement and ground-surface settlement caused by pit-in-pit foundation pit in soft clays. *KSCE Journal of Civil Engineering*, *25*(4), 1262–1275. https://doi.org/10.1007/s12205-021-1120-8

Tong, L., Li, H., Ha, S., & Liu, S. (2021). Lateral bearing performance and mechanism of piles in the transition zone due to pit-in-pit excavation. *Acta Geotechnica*, *17*(5), 1935–1948. https://doi.org/10.1007/s11440-021-01341-3

Wang, J. H., Xu, Z. H., & Wang, W. D. (2010). Wall and ground movements due to deep excavations in Shanghai soft soils. *Journal of Geotechnical and Geoenvironmental Engineering*, *136*(7), 985–994. https://doi.org/10.1061/(ASCE)GT.1943-5606.0000299

Zeng, C.-F., Xue, X.-L., Zheng, G., Xue, T.-Y., & Mei, G.-X. (2018). Responses of retaining wall and surrounding ground to pre-excavation dewatering in an alternated multi-aquifer-aquitard system. *Journal of Hydrology*, *559*, 609–626. https://doi.org/10.1016/j.jhydrol.2018.02.069

Zhang, Y.-Q., Li, M.-G., Wang, J.-H., Chen, J.-J., & Zhu, Y.-F. (2017). Field tests of pumping-recharge technology for deep confined aquifers and its application to a deep excavation. *Engineering Geology*, *228*, 249–259. https://doi.org/10.1016/j.enggeo.2017.08.019

Zheng, G., Li, Q. H., Cheng, X. S., Ha, D., Shi, J. C., Shi, X. R., & Lei, Y. W. (2022). Diaphragm wall deformation and ground settlement caused by dewatering before excavation in strata with leaky aquifers. *Géotechnique*, *74*(1), 1–17. https://doi.org/10.1680/jgeot.21.00038

Zheng, G., & Wei, S. W. (2008). Numerical analyses of influence of overlying pit excavation on existing tunnels. *Journal of Central South University of Technology*, *15*, 69–75. https://doi.org/10.1007/s11771-008-0438-4

Zhou, N., Vermeer, P. A., Lou, R., Tang, Y., & Jiang, S. (2010). Numerical simulation of deep foundation pit dewatering and optimization of controlling land subsidence. *Engineering Geology*, *114*(3–4), 251–260. https://doi.org/10.1016/j.enggeo.2010.05.002